Numerical investigation of interaction of two internal solitary waves with different initial wave amplitudes

Yingjie Hu [1], Zongbing Yu [2] *, Li Zou [2, 3], Xinyu Ma [2]

[1] Department of Hydraulic Engineering, Tsinghua University, Beijing, 100084, China

[2] School of Naval Architecture, State Key Laboratory of Structural Analysis, Optimization and CAE Software for Industrial Equipment, Dalian University of Technology, Dalian 116024, China

[3] Southern Marine Science and Engineering Guangdong Laboratory (Guangzhou), Guangzhou 511458, China

* yuzb@dlut.edu.cn

Abstract. The present study investigates the collision of two internal solitary waves with different initial amplitudes using a multi-domain boundary element method. It calculates and discusses wave profiles, residence time, and phase shifting. Observations reveal that tail waves are induced during the collision process, with the amplitude of the tail wave increasing as the initial amplitude of the internal solitary wave increases. Residence time, defined in terms of the interaction between waves of different initial amplitudes, decreases as wave amplitudes increase, eventually stabilizing at a constant value. Additionally, phase shifting increases with wave amplitude, with the rate of increase slowing down as the wave profile becomes relatively large.

Keywords: Internal solitary wave; collision; boundary element method; potential flow.

1. Introduction

Due to the frequent occurrence of internal solitary waves in the ocean[1-3], multiple internal solitary waves or wave trains often coexist in the same region. However, interactions between these waves can substantially amplify wave amplitudes and induce dramatic changes in the flow field, thereby increasing their destructive potential. Furthermore, these interactions alter the propagation and evolution characteristics of internal solitary waves, underscoring the importance of studying their interactions in ocean dynamics research.

Regarding the interaction issues during collisions of two internal solitary waves, some scholars have derived relevant analytical models. Mirie and Su [4-5] utilized a perturbation method capable of generating asymptotic analytical solutions of all orders to study head-on collisions between two solitary waves in inviscid homogeneous fluids. Gear [6] analytically studied the interaction of two internal solitary waves using coupled KdV equations. Conditions for weak and strong interactions were discussed, and computational results for both interactions were presented, analyzing the evolution characteristics of internal solitary waves. Yuan et al. [7] investigated the wave-wave interactions between two obliquely propagating internal solitary waves influenced by topography based on the variable-coefficient KP equation. Numerical simulation studies of internal solitary wave interactions have garnered scholarly attention. Cooker [8] utilized a boundary integral method to investigate collisions between surface solitary waves propagating over a horizontal seabed and a vertical wall. The study analyzed the motion characteristics as solitary waves approached the wall and phase shifts during both small and large amplitude wave reflection processes. Javam et al. [9] employed two momentum sources to study wave-wave interactions between two wave rays, discovering that nonlinear interactions between internal waves can lead to wave breaking phenomena. Jo and Choi [10] numerically investigated a strong nonlinear asymptotic model describing the evolution of large amplitude internal waves in a two-layer system.

As an efficient numerical method based on potential flow theory, boundary element method has been applied in the simulation of water wave widely. However, the calculation of the interaction of two internal solitary waves with different amplitude based on boundary element method has rarely

been studied. In present study, multi-domain boundary element method is adopted to investigate the collision of nonlinear internal solitary waves.

2. Method

The fluid in computational domain is assumed to be no viscous, nonrotational and incompressible, thus the fluid velocities u_k can be expressed as the gradient of the potentials ϕ_k. The velocity potentials in two-layer fluids satisfy Laplace equation

$$\nabla^2\phi_k = 0 \quad k = 1,\ 2. \tag{1}$$

The interface of two-layer fluids satisfies kinetic condition (2) and dynamic condition (3).

$$\frac{\partial\phi_1}{\partial\mathbf{n}} = \frac{\partial\phi_2}{\partial\mathbf{n}} \quad on\ \ z = \eta_2(x,t). \tag{2}$$

$$\rho_1\left(\frac{\partial\phi_1}{\partial t} + \frac{1}{2}\left|\nabla\phi_1\right|^2 + g\eta_2\right) = \rho_2\left(\frac{\partial\phi_2}{\partial t} + \frac{1}{2}\left|\nabla\phi_2\right|^2 + g\eta_2\right) \quad on\ z = \eta_2(x,t). \tag{3}$$

The impenetrable boundary condition at the rigid seabed requires

$$\frac{\partial\phi_2}{\partial n} = 0 \ \ on\ z = -h_2. \tag{4}$$

The top of the upper liquid layer is a free surface, where the kinematic and dynamic boundary conditions are

$$\frac{D\boldsymbol{r}_1}{Dt} = \nabla\phi_1 \quad on\ z = h_1 + \eta_1(x,t), \tag{5}$$

$$\frac{\partial\phi_1}{\partial t} + \frac{1}{2}\left|\nabla\phi_1\right|^2 + g\eta_1 = 0 \quad on\ z = h_1 + \eta_1, \tag{6}$$

where $\boldsymbol{r}_1$ is the position of top free surface.

Governing equations in the upper layer Ω_1 and lower layer Ω_2 can be converted into boundary integral equations (7) at boundaries Γ_1 and Γ_2 based on Green's second identity.

$$c(\mathbf{r})\varphi_k(\mathbf{r}) = \int_{\Gamma_k}\left(\varphi_k(\mathbf{q})\frac{\partial G(\mathbf{r},\mathbf{q})}{\partial n} - G(\mathbf{r},\mathbf{q})\frac{\partial\varphi_k(\mathbf{q})}{\partial n}\right)dl(\mathbf{q}), \tag{7}$$

where r is the field point, q is the source point, $G(\mathbf{r},\mathbf{q}) = \frac{1}{2\pi}\ln\frac{1}{|\mathbf{r}-\mathbf{q}|}$ is the Green function, and c(r) is the solid angle of the boundary at point r.

The boundary integral equation (7) is solved numerically based on MDBEM. Both boundaries Γ_1 and Γ_2 are discretized into n elements Γ_{ij} from point $\mathbf{q}_j$ to $\mathbf{q}_{j+1}$. Thus equation (7) can be expressed as the discrete form as equation (8)

$$c(\mathbf{r})\varphi_i(\mathbf{r}) = -\sum_{j=1}^{n}\left(\varphi_k(\mathbf{r}_j)\int_{\Gamma_{kj}}\frac{\partial G(\mathbf{r},\mathbf{q})}{\partial n}dl(\mathbf{q})\right) + \sum_{j=1}^{n}\left(\psi_k(\mathbf{r}_j)\int_{\Gamma_{kj}}G(\mathbf{r},\mathbf{q})dl(\mathbf{q})\right). \tag{8}$$

3. Results

The evolution of waveforms during the head-on collision interaction of two internal solitary waves with different amplitudes is shown in Figure 1. In contrast to interactions involving internal solitary waves of the same amplitude, during interactions between two solitary waves of different amplitudes, the position of maximum wave amplitude no longer occurs at the center but rather shifts towards the side of the smaller amplitude solitary wave. This is because the larger amplitude solitary wave propagates faster than the smaller amplitude solitary wave, causing the interaction position to shift away from the center. From the figure, it can be observed that the maximum amplitude of the trailing wave generated during the interaction of two internal solitary waves is correlated with the initial wave amplitudes of the solitary waves; the larger the amplitude of the internal solitary wave, the larger the maximum amplitude of the trailing wave generated. A three-dimensional plot of non-equal-height internal solitary wave collisions is shown in Figure 2.

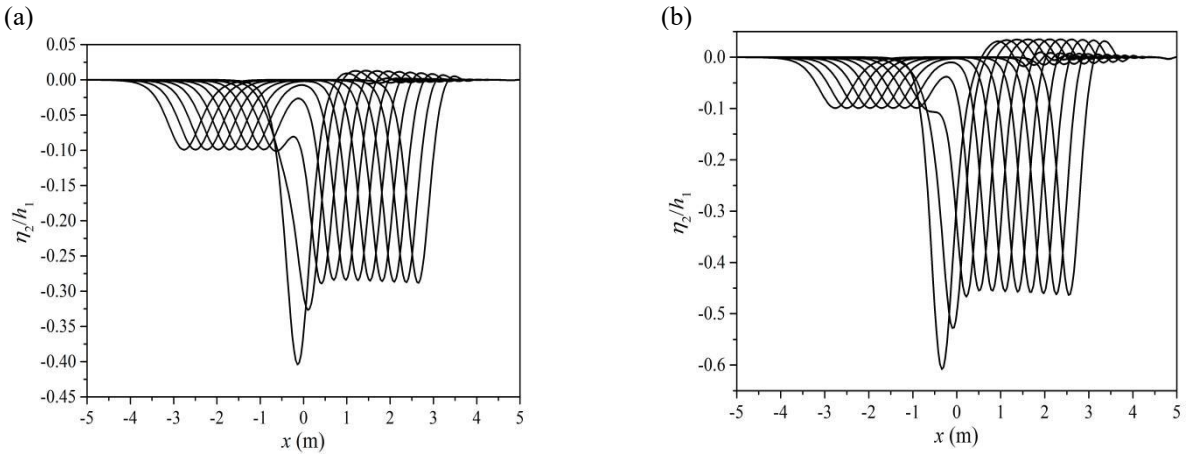

Fig. 1 The wave profile variation in the collision process of two internal solitary waves with different amplitudes

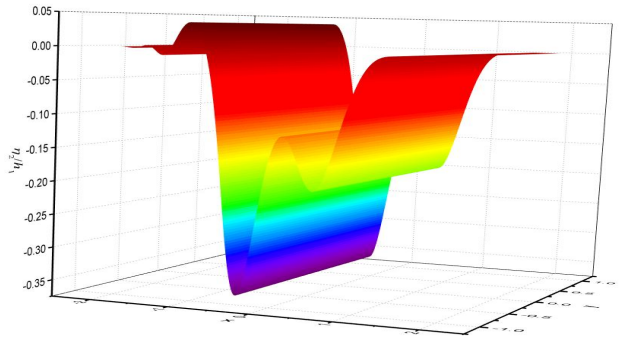

Fig. 2 The three-dimensional figure of the collision of two internal solitary waves with different amplitudes

Due to the distinct waveform characteristics between the wave-wave interaction of two unequal-amplitude internal solitary waves and the head-on collision of equal-amplitude internal solitary waves, this paper has redefined the concept of stagnation time in the context of unequal-amplitude internal solitary wave collisions, as illustrated in Figure 3.

$$t_{rc} = t_s - t_f \tag{9}$$

Where, t_f denotes the initial time when two internal solitary waves have just merged into a single trough during their collision process, and t_s represents the final moment before a single trough separates into two troughs. Therefore, in this paper, the stagnation time during the collision of two unequal-amplitude internal solitary waves refers to the duration during which two waveforms remain merged into a single trough.

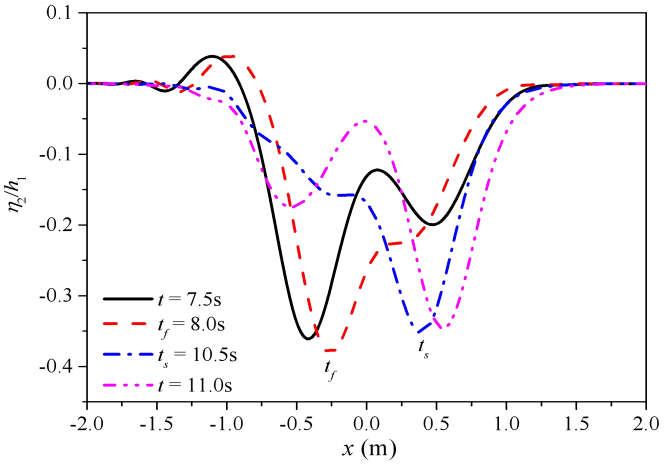

Fig. 3 The definition of residence time for the collision of two internal solitary waves with different amplitude

The resident time during the head-on collision of two internal solitary waves with different amplitudes varies with wave amplitude, as shown in Figure 4 The left internal solitary wave maintains a dimensionless wave amplitude of a1/h1 = 0.4 throughout, while the right internal solitary wave has dimensionless wave amplitudes of a1/h1 = 0.2，0.3，0.4，0.5，0.6. From the graph, it can be observed that during the collision of two internal solitary waves, when one wave's amplitude is fixed, the stagnation time decreases as the amplitude of the other internal solitary wave increases. For smaller amplitudes (a1/h1 = 0.2), the stagnation time significantly decreases with increasing amplitude, whereas after reaching a certain value (a1/h1 = 0.5), the change in stagnation time becomes smaller and stabilizes. Figure 5 illustrates the difference between the maximum amplitude achieved during collisions of internal solitary waves with different amplitude combinations and the result from linear superposition. As the initial amplitude increases, the difference between the maximum amplitude and the linear superposition result significantly increases.

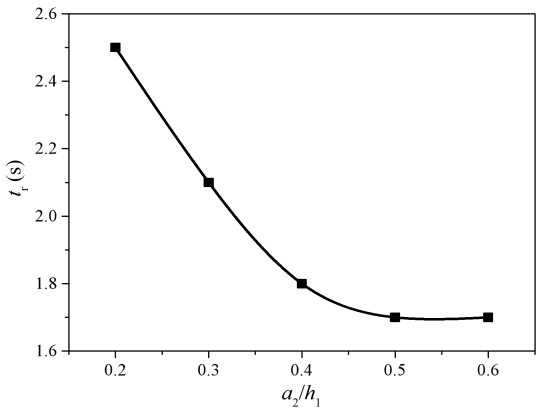

Fig.4 The residence time for the collision of two internal solitary waves

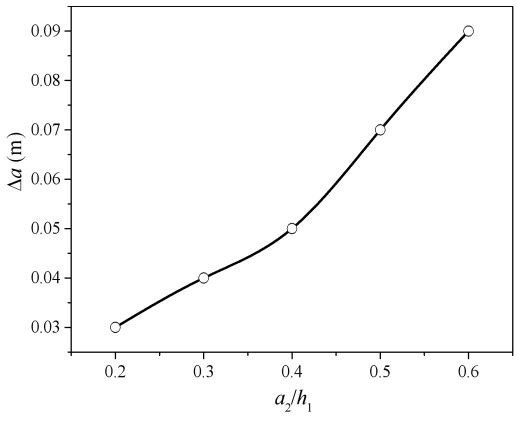

Fig.5 The maximum run up error between linear results and the calculation results

To validate the accuracy of the numerical model in calculating phase shift characteristics, the computed results are compared with those from reference [2], as shown in Figure 6(a). This comparison demonstrates that the method proposed in this paper accurately computes the phase shift characteristics during collisions of internal solitary waves. Figure 6(b) illustrates the phase lag produced during collisions of internal solitary waves with different initial amplitudes when the density ratio ρ1/ρ2 = 856/996. It can be observed that the phase shift generated during the collision process significantly increases with larger initial amplitudes, and the rate of increase gradually diminishes.

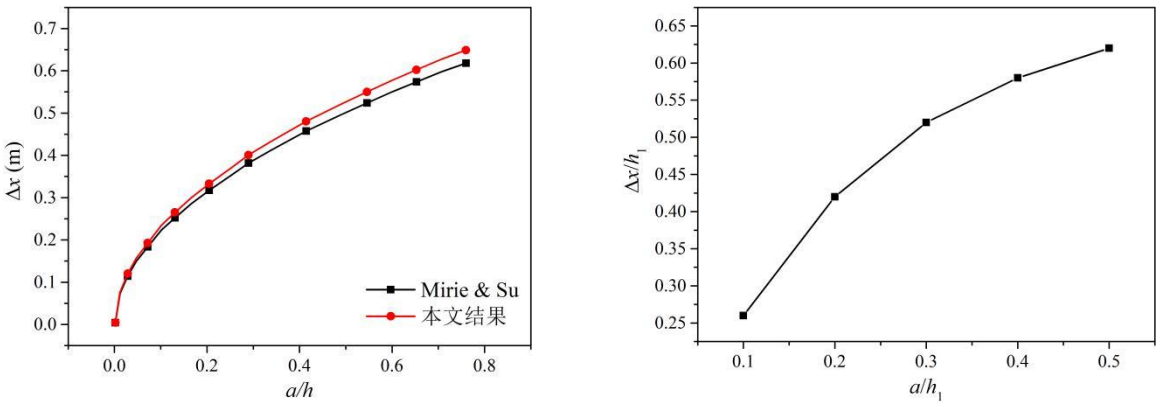

(a) (b)

Fig. 6 The phase shifting during the collision of two internal solitary waves with the literature, (a) The comparison with literature, (b) The calculation results for the present cases

4. Conclusions

The present paper studies the collision of two internal solitary waves with different initial amplitudes based on potential flow theory in stratified fluids. It can be found that tail waves are induced during the collision process, with the amplitude of the tail wave increasing as the initial amplitude of the internal solitary wave increases. Residence time, defined in terms of the interaction between waves of different initial amplitudes, decreases as wave amplitudes increase, eventually stabilizing at a constant value. Additionally, phase shifting increases with wave amplitude, with the rate of increase slowing down as the wave profile becomes relatively large.

Acknowledgement

This work was supported by Hunan Provincial Natural Science Foundation of China (2021JC0010)， Research Fund from National Key Laboratory of Autonomous Marine Vehicle Technology (2022JCJQ-SYSJJ-LB06901) National Natural Science Foundation of China (52301375).

References

[1] Helfrich K. R., Melville W. K. Long nonlinear internal waves[J]. Annual Review of Fluid Mechanics, 2006, 38: 395-425.

[2] Stanton T. P., Ostrovsky L. A. Observations of highly nonlinear internal solitons over the continental shelf[J]. Geophysical Research Letters, 1998, 25(14): 2695-2698.

[3] Magalhaes J. M., Da Silva B J. C. Internal solitary waves in the Andaman Sea: new insights from SAR imagery[J]. Remote Sensing, 2018, 10(8616).

[4] Mirie R. M., Su C. H. Collisions between two solitary waves. Part 2. A numerical study[J]. Journal of Fluid Mechanics, 1982, 115(-1): 475.

[5] Mirie R. M., Su C. H. Internal solitary waves and their head-on collision. Part 1[J]. Journal of Fluid Mechanics, 1984, 147(-1): 213.

[6] Gear J. A., Grimshaw R. Weak and Strong Interactions between Internal Solitary Waves[J]. Studies in Applied Mathematics (Cambridge), 1984, 70(3): 235-258.

[7] Yuan C., Grimshaw R., Johnson E., Wang Z. Topographic effect on oblique internal wave – wave interactions[J]. Journal of Fluid Mechanics, 2018, 856: 36-60.

[8] Cooker M. J., Weidman P. D., Bale D. S. Reflection of a high-amplitude solitary wave at a vertical wall[J]. Journal of Fluid Mechanics, 1997, 342: 141-158.

[9] Javam A., Imberger J., Armfield S. W. Numerical study of internal wave-wave interactions in a stratified fluid[J]. Journal of Fluid Mechanics, 2000, 415: 65-87.

[10] Jo T. C., Choi W. On stabilizing the strongly nonlinear internal wave model[J]. Studies in Applied Mathematics, 2008, 201(1): 65–85.